Effects of Antenna Patterns on Cloud Radar Polarimetric Measurements

ALEXANDER MYAGKOV, PATRIC SEIFERT, AND ULLA WANDINGER

Leibniz Institute for Tropospheric Research (TROPOS), Leipzig, Germany

MATTHIAS BAUER-PFUNDSTEIN

METEK GmbH, Elmshorn, Germany

SERGEY Y. MATROSOV

Cooperative Institute for Research in Environmental Sciences, University of Colorado, and NOAA/Earth System Research Laboratory/Physical Sciences Division, Boulder, Colorado

(Manuscript received 22 February 2015, in final form 29 May 2015)

ABSTRACT

This paper presents an experimental analysis of the antenna system effects on polarimetric measurements conducted with cloud radars operating in the linear depolarization ratio (LDR) mode. Amplitude and phase of the copolar and cross-polar antenna patterns are presented and utilized. The patterns of two antennas of different quality were measured at the Hungriger Wolf airport near Hohenlockstedt, Germany, during the period from 28 January to 1 February 2014. For the measurements a test transmitter mounted on a tower and the scanning 35-GHz (Ka band) cloud radar MIRA-35, manufactured by METEK GmbH and operated in the receiving mode, were used. The integrated cross-polarization ratios (ICPR) are calculated for both antennas and compared with those measured in light rain. Correction algorithms for observed LDR and the co-cross-channel correlation coefficient ρ are presented. These algorithms are aimed at removing/mitigating polarization cross-coupling effects that depend on the quality of radar hardware. Thus, corrected LDR and ρ are primarily influenced by scatterer properties. The corrections are based on the decomposition of the coherency matrix of the received signals into fully polarized and nonpolarized components. The correction brings LDR values and the co-cross-channel correlation coefficients from two radars with different antenna systems to a close agreement, thus effectively removing hardware-dependent biases. Uncertainties of the correction are estimated as 3 dB for LDR in the range from −30 to −10 dB. In clouds, the correction of the co-cross-channel correlation coefficient ρ results in near-zero values for both vertically pointed radars.

1. Introduction

Cloud radar is an important tool for active remote sensing of atmospheric hydrometeors. Measurements from cloud radars, which are typically operated at Ka-band (~35 GHz) or W-band (~94 GHz) frequencies, are nowadays widely used, often in combination with other active and passive remote sensing instruments, for retrieving cloud microphysical and macrophysical properties (Illingworth et al. 2007; Kollias et al. 2007; Shupe et al. 2008). In addition to standard radar variables (e.g., the moments of the Doppler spectrum), which are usually used for estimations of cloud water content and characteristic sizes and number concentrations of cloud particles (Donovan and van Lammeren 2001; Eloranta et al. 2007; Rambukkange et al. 2011), cloud radars also often have polarization capabilities that provide additional possibilities for hydrometeor-type classification and shape estimation (Matrosov 1991). Polarimetric radar methods have also been shown to be efficient for detecting hazardous weather phenomena (Ryzhkov et al. 2005b), classification of precipitation (Ryzhkov et al. 2005a; Park et al. 2009), and estimation of microphysical

Denotes Open Access content.

Corresponding author address: Alexander Myagkov, Remote Sensing of Atmospheric Processes, Leibniz Institute for Tropospheric Research (TROPOS), Permoserstraße 15, 04318 Leipzig, Germany.
E-mail: myagkov@tropos.de

DOI: 10.1175/JTECH-D-15-0045.1

properties (Ryzhkov et al. 2005a). Advantages of polarimetric methods for cloud radars were investigated previously by Lohmeier et al. (1997), Matrosov et al. (2001), Wolde and Vali (2001a), Wolde and Vali (2001b), and Matrosov et al. (2012).

Many commercially produced cloud radars operate in the linear depolarization ratio (LDR) mode. In this mode the radar transmits electromagnetic waves with a horizontal polarization state and receives both horizontal and vertical polarization components of the scattered wave in the co- and cross channels, respectively. In this paper we consider cloud radars with two receiving channels that allow simultaneous measurements of copolarized and cross-polarized components of backscatter signals. The LDR mode permits detecting the melting layer (Di Girolamo et al. 2012) and distinguishing between cloud and insect echoes (Martner and Moran 2001). The main disadvantage of this polarimetric measurement mode is a low signal-to-noise ratio (SNR) in the cross channel (Matrosov and Kropfli 1993). This disadvantage leads to two problems. The first problem is that at some ranges the backscatter signals in the cross channel are too low to be detected. In this case, there is no polarimetric information available. We do not consider this problem in this paper. The second problem is the polarization coupling (or leakage) that occurs in the waveguide transmission line, the orthomode transducer, and the antenna (further, we denote all the mentioned parts as the antenna system) because radar hardware is never ideal. A fraction of the received cochannel signal leaks into the cross channel. This effect determines the minimal LDR value, which varies from radar to radar depending on hardware characteristics. This leads to the fact that LDR values, which are observed from hydrometeor populations with the same microphysical properties, will differ for different radars (Matrosov 2015). It complicates depolarization measurement interpretations; thus, it is desirable to remove/mitigate differing hardware effects from such measurements. If the hardware effects are removed from LDR measurements, then these measurements can be more effectively used to infer hydrometeor properties that influence LDR (e.g., particle shape and orientation characteristics).

When measurements of the phase relations between signals in the radar polarimetric channels in the LDR mode are available, a so-called correlation coefficient ρ can be calculated. This parameter [denoted as the co-cross-polar correlation coefficient in Ryzhkov (2001)] contains additional information about meteorological scatterers, such as a mean axis ratio of particles and parameters describing the orientation distribution of scatterers (Ryzhkov 2001). However, ρ is also influenced by the polarimetric properties of the radar hardware (Galletti et al. 2014).

The antenna system's influence on radar polarimetric measurements has been investigated in a number of studies. For instance, Chandrasekar and Keeler (1993) performed a theoretical study of the errors introduced by complex antenna patterns on the measurements of LDR, differential reflectivity (Z_{DR}), and differential phase shift. These authors, however, considered only measurements of the amplitude antenna patterns and defined the accuracy bounds for the radar variables mentioned above. Mudukutore et al. (1995) described a technique for measurements of the differential phase antenna pattern and investigated the influence of this pattern on the differential phase shift and the cross-correlation coefficient ρ_{hv} measured with weather radars that operate with pulse-to-pulse switching of the transmitted polarization state (Bringi and Chandrasekar 2001). Bringi and Chandrasekar (2001) provide a review of different studies focusing on antenna influences on polarimetric variables in different radar configurations. Zrnić et al. (2010) considered the influence of a bias in Z_{DR} produced by the antenna on rain-rate estimations. Frech et al. (2013) conducted measurements of amplitude and phase antenna patterns in order to estimate the influence of a radome on polarimetric observations with weather radars.

It was shown in Kanareykin et al. (1968) that the basis of the electromagnetic wave coherency matrix can be changed by applying the unitary matrix transformation in such a way that the orthogonal components of the wave are not correlated. This transformation is known as the second specific basis of the coherency matrix (Kanareykin et al. 1968). The effectiveness of this transformation for the correction of the coherent coupling was recently shown (Galletti 2013; Galletti et al. 2014). It is noted that noncoherent leakage cannot be removed with this method.

In this paper we describe a correction approach to remove/mitigate the hardware effects in LDR and the correlation coefficient measurements based on the complex antenna pattern data and the coherency matrix decomposition. For this study cloud radars of the type MIRA-35 were used. MIRA-35 (Görsdorf et al. 2015) is a Ka-band (35 GHz) Doppler cloud radar that is produced by METEK GmbH. It is used at more than 10 measurement sites within Europe for cloud studies. The main technical specifications of a typical MIRA-35 radar are listed in Table 1.

The paper is organized as follows. Section 2 contains theoretical considerations to describe the antenna system's patterns, the description of the instrumentation,

TABLE 1. Parameters of MIRA-35 used in the operational mode.

Peak power (kW)	30
Pulse length (ns)	200
Pulse repetition frequency (kHz)	5
Minimum range (km)	0.15
Maximum range (km)	15
Range resolution (m)	30
No. of pulses for FFT	256
No. of spectra for averaging	200
Sensitivity at 5 km (dBZ)	−55

and the measurement results. The application of the coherency matrix for the correction of LDR and the correlation coefficient is shown in section 3. Conclusions and further considerations are presented in section 4.

2. Measurements of complex antenna patterns

a. Problem definition

Any polarization analysis requires a choice of the reference polarization basis. Usually the orthogonal linear basis ($\mathbf{e}_x$ $\mathbf{e}_y$), formed by two unit vectors defined by the antenna feeders, is used. Generally, vectors $\mathbf{e}_x$ and $\mathbf{e}_y$ correspond to the horizontal and vertical polarization states, respectively. In the LDR mode used by many cloud radars, the horizontal component of the wave is received in the cochannel of the radar and the vertical one is received in the cross channel. The complex amplitudes of the received pulses in the co- and cross channels can be described by

$$\dot{E}_x = E_x \exp(i\Phi_x) \quad \text{and} \tag{1}$$

$$\dot{E}_y = E_y \exp(i\Phi_y), \tag{2}$$

where E_x, Φ_x and E_y, Φ_y are amplitudes and phases of the received pulses in the co- and cross channels, respectively. The dot over an identifier letter hereafter represents a complex quantity.

The polarimetric parameter LDR is the ratio of the received powers in the co- and cross channels and can be calculated in linear units as

$$\mathrm{LDR} = \frac{\langle E_y^2 \rangle}{\langle E_x^2 \rangle}, \tag{3}$$

where the angle brackets ($\langle\ \rangle$) denote averaging over a number of pulses. Afterward, we use linear scales of LDR in equations, while logarithmic scales expressed in decibels are used for values in figures and discussion. We denote scatterers with the unity backscattering matrix as isotropic particles. Note, that not only spherical

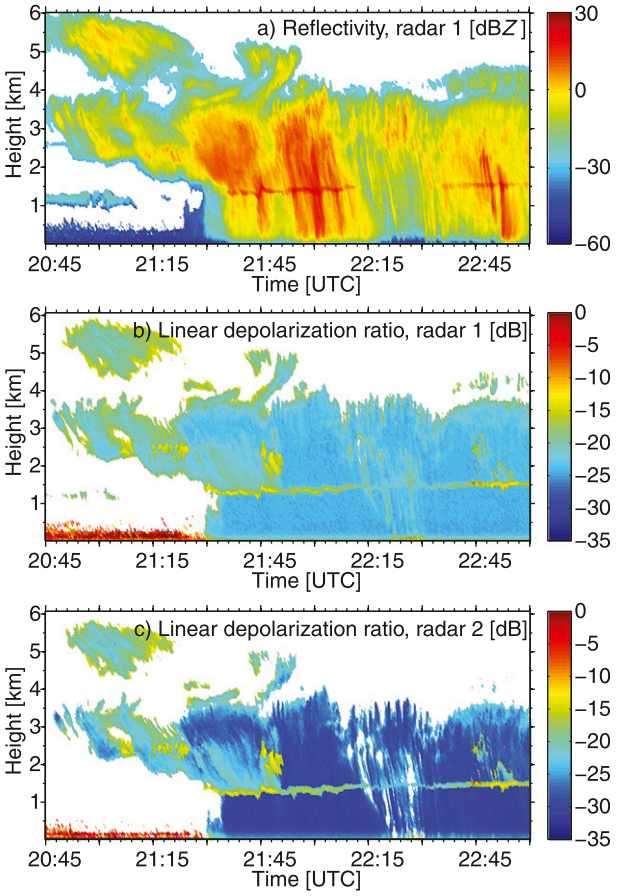

FIG. 1. Time–height cross section of observed parameters: (a) Reflectivity for radar 1; (b) LDR for radar 1; and (c) LDR for radar 2, taken at Elmshorn, Germany, on 8 Nov 2013. Please note that the amount of data points in (c) is less in comparison with (b) because of the lower sensitivity of radar 2.

scatterers but also horizontally aligned oblate spheroids and plates can be considered as isotropic when observed by a vertically pointed radar. Even though the theoretical value of LDR in the logarithmic scale for isotropic particles is $-\infty$, the measured values are always finite and they depend on radar hardware and noise. Figure 1 shows the equivalent reflectivity factor (hereafter just reflectivity) and LDR measurements obtained with two collocated vertically pointed MIRA-35 cloud radars that were tested at the METEK site. We denote these radars as "radar 1" and "radar 2." The distance between the radars was about 30 m. A precipitating cloud system that passed over the METEK site was simultaneously observed by both radars. The melting layer, indicated by a region of increased reflectivity and LDR, can be seen at heights between 1.3 and 1.5 km. Reflectivity values of approximately 30 dBZ observed below the melting layer correspond to light rain (Straka et al. 2000). For vertically viewing cloud radars, the polarimetric

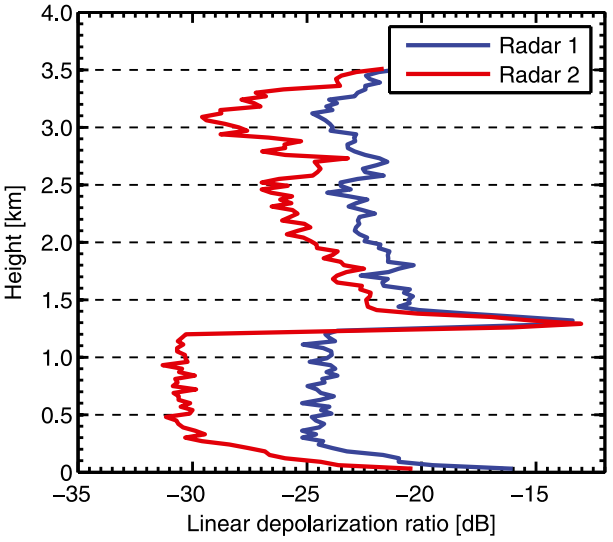

FIG. 2. Vertical profiles of LDR for radars 1 and 2 at 2140 UTC 8 Nov 2013 (for the same case as in Fig. 1).

variables of raindrops can be described by a population of particles with isotropic polarimetric scattering properties. Therefore, this measurement case was chosen for the comparison of minimal LDR values.

Figures 1b and 1c show similar patterns of LDR for both radars. Nevertheless, the values of LDR are significantly different. In Fig. 2 the vertical profiles of LDR measured by both radars at 2140 UTC are presented. The antenna system of radar 1 results in minimal LDR values of about −25 dB and the antenna system of radar 2 causes minimal LDR values of approximately −31 dB. Further, we will denote the antenna of radar 1 as "bad" and the antenna of radar 2 as "good." Note that even though the minimal LDR differs for both systems, the LDR produced by the melting layer is approximately the same because the signal in the cross channel in this layer is mostly determined by scattering from melting particles and not by the polarization leakage.

Another example of the antenna system's influence on the polarimetric measurements is given by Matrosov et al. (2012), who evaluated the implementation of the slanted LDR mode (SLDR mode) into a cloud radar. The SLDR mode can be implemented starting from the LDR mode by rotation of the radar antenna by 45°. The authors noticed that due to the antenna rotation, the minimal LDR value increased compared to the minimal LDR value observed in LDR mode. Increased values of minimal LDR can mask less-pronounced depolarizing structures in the data. In addition, variations in the minimal LDR of different radar systems reduce the comparability of respective measurements of LDR.

In general, the full set of receiving antenna patterns can be presented in matrix form:

$$\mathbf{F}(\theta,\phi)=\begin{bmatrix}\dot{f}_{xx}(\theta,\phi) & \dot{f}_{yx}(\theta,\phi)\\ \dot{f}_{xy}(\theta,\phi) & \dot{f}_{yy}(\theta,\phi)\end{bmatrix}, \tag{4}$$

where $\dot{f}_{mn}(\theta, \phi)$ are complex antenna patterns. The first index m describes the polarization state of the wave incident on the antenna (either horizontal or vertical); the second index n describes the polarization of the receiving channel; and θ and ϕ represent the azimuth and elevation angles of the received wave with respect to the maximum of the radar beam, respectively.

The minimal LDR value for a particular radar is sometimes denoted as the integrated cross-polarization ratio (ICPR). Chandrasekar and Keeler (1993) showed that ICPR can be calculated from the antenna patterns. In terms of the receiving antenna patterns [Eq. (4)], ICPR can be written as follows:

$$\mathrm{ICPR}=\frac{\int|\dot{f}_{xx}(\theta,\phi)\dot{f}_{xy}(\theta,\phi)+\dot{f}_{yx}(\theta,\phi)\dot{f}_{yy}(\theta,\phi)|^2\,d\Omega}{\int|\dot{f}^2_{xx}(\theta,\phi)+\dot{f}^2_{yx}(\theta,\phi)|^2\,d\Omega}, \tag{5}$$

where $d\Omega$ is the elemental solid angle and the integration is performed over the 4π solid angle.

Equation (5) can be represented as a sum of three components:

$$P_1=\frac{|\dot{f}_{xx}(\theta,\phi)|^2|\dot{f}_{xy}(\theta,\phi)|^2}{\int|\dot{f}^2_{xx}(\theta,\phi)+\dot{f}^2_{yx}(\theta,\phi)|^2\,d\Omega}, \tag{6}$$

$$P_2=\frac{|\dot{f}_{yx}(\theta,\phi)|^2|\dot{f}_{yy}(\theta,\phi)|^2}{\int|\dot{f}^2_{xx}(\theta,\phi)+\dot{f}^2_{yx}(\theta,\phi)|^2\,d\Omega}, \quad \text{and} \tag{7}$$

$$P_3=\frac{2\mathrm{Re}[\dot{f}_{xx}(\theta,\phi)\dot{f}^*_{xy}\,(\theta,\phi)\dot{f}_{yx}(\theta,\phi)\dot{f}^*_{yy}\,(\theta,\phi)]}{\int|\dot{f}^2_{xx}(\theta,\phi)+\dot{f}^2_{yx}(\theta,\phi)|^2\,d\Omega}, \tag{8}$$

where the asterisk (*) is the complex conjugation sign. Note in Eqs. (6) and (7) that the calculation of the components P_1 and P_2 does not require complex antenna patterns. The phase relations appear only in P_3.

Using the approach of Chandrasekar and Keeler (1993) and taking into account that $|\dot{f}_{yx}(\theta, \phi)| \ll |\dot{f}_{xx}(0, 0)|$, the bias in the correlation coefficient can be written as follows:

$$\rho_b = \frac{\left| \int [\dot{f}_{xx}(\theta,\phi)^3 \dot{f}_{xy}(\theta,\phi) + \dot{f}_{xx}(\theta,\phi)^2 \dot{f}_{yx}(\theta,\phi)\dot{f}_{yy}(\theta,\phi)]\, d\Omega \right|}{\left[\int |\dot{f}_{xx}(\theta,\phi)\dot{f}_{xy}(\theta,\phi) + \dot{f}_{yx}(\theta,\phi)\dot{f}_{yy}(\theta,\phi)|^2\, d\Omega \int |\dot{f}_{xx}^2(\theta,\phi)|^2\, d\Omega \right]^{1/2}}. \tag{9}$$

We further introduce the following parameters:

$$R_1 = \frac{\mathrm{Re}\{[\dot{f}_{xx}(\theta,\phi)^3 \dot{f}_{xy}(\theta,\phi) + \dot{f}_{xx}(\theta,\phi)^2 \dot{f}_{yx}(\theta,\phi)\dot{f}_{yy}(\theta,\phi)]\}}{\left[\int |\dot{f}_{xx}(\theta,\phi)\dot{f}_{xy}(\theta,\phi) + \dot{f}_{yx}(\theta,\phi)\dot{f}_{yy}(\theta,\phi)|^2\, d\Omega \int |\dot{f}_{xx}^2(\theta,\phi) + \dot{f}_{yx}^2(\theta,\phi)|^2\, d\Omega \right]^{1/2}} \quad \text{and} \tag{10}$$

$$R_2 = \frac{\mathrm{Im}\{[\dot{f}_{xx}(\theta,\phi)^3 \dot{f}_{xy}(\theta,\phi) + \dot{f}_{xx}(\theta,\phi)^2 \dot{f}_{yx}(\theta,\phi)\dot{f}_{yy}(\theta,\phi)]\}}{\left[\int |\dot{f}_{xx}(\theta,\phi)\dot{f}_{xy}(\theta,\phi) + \dot{f}_{yx}(\theta,\phi)\dot{f}_{yy}(\theta,\phi)|^2\, d\Omega \int |\dot{f}_{xx}^2(\theta,\phi) + \dot{f}_{yx}^2(\theta,\phi)|^2\, d\Omega \right]^{1/2}}. \tag{11}$$

Integrating the components $P_{1,2,3}$ and $R_{1,2}$ over specific areas of the antenna patterns can indicate from where most of the coupling between the co- and cross channels comes.

Antenna manufacturers usually provide only information about two amplitude cut planes, $|\dot{f}_{xx}(\theta, 0)|$ and $|\dot{f}_{xx}(0, \phi)|$, which is not sufficient for the analysis of the antenna system's influence on polarimetric variables. Therefore, measurements of the complex antenna pattern were performed for two different antennas with good and bad polarimetric characteristics, respectively.

b. *Measurement description*

The antenna pattern measurements were performed as described by Chandrasekar and Keeler (1993) and Mudukutore et al. (1995). The field experiment was conducted at the Hungriger Wolf airport near Hohenlockstedt (53.993°N, 9.577°E), Germany, during the period from 28 January to 1 February 2014. The cloud radar MIRA-35, denoted as radar 1 in section 2a, was used for the measurements. The radar was equipped with a scanning unit (Fig. 3) based on drives of type Aerotech AGR200 with a high gear ratio. The scanning unit allows for changing the azimuth angle between 0° and 360° and the elevation angle between 0° and 180° with a resolution of 0.034°. Two different Cassegrain dual-reflector antennas were taken for the measurements. They were denoted as bad and good antennas in section 2a. Both antennas were installed to the same transceiver unit of radar 1. The antenna specifications as provided by the manufacturer are listed in Table 2.

In general, the moments of the Doppler spectra measured with MIRA-35 are used to derive information about the cloud properties. The phase relations between co- and cross channels are not saved. Nevertheless, the receiver unit of the radar allows for saving in-phase (I) and quadrature (Q) components of the received signal in both polarization channels. The quadrature components make it possible to obtain not only the amplitude of the signals but also their phase. Therefore, during the antenna pattern measurements, the radar was operating in the receiving mode (the transmitter unit was turned off) and the receiving antenna patterns were measured consecutively with the good and the bad antennas.

A custom-made test transmitter was used for generation of the continuous wave at Ka band. The test transmitter consists of a continuous-wave X-band generator with software-based frequency control, a 4-times frequency multiplier, and an antenna system based on a pyramidal horn antenna. The horn antenna forms a linearly polarized wave. As the antenna system of the test transmitter allows for rotation of the horn, it is possible to change manually the orientation angle β in the polarization plane of the transmitted wave with respect to the x axis of the radar polarization basis. The output power of the test transmitter is 4 mW.

Basically, the bistatic measurements of the absolute phase require high stability of the local oscillators of the transmitter and the receiver. The local oscillators that are used in the radar receiver and the test transmitter are based on quartz resonators and cannot be used for long-term phase measurements due to the frequency drift. The short-term stability (Allan deviation over 1 s) of quartz resonators is on the order of 10^{-9} (Vig 1992), which allows for performing phase measurements only for short time periods, as the local oscillators can be assumed coherent in this case. Therefore, only the phase differences between polarization channels were calculated in addition to the amplitudes. Moreover, the absolute phases are not necessary for the modeling of

FIG. 3. The MIRA-35 cloud radar with the scanning unit at METEK GmbH. The photo was provided by METEK GmbH.

scattering properties of meteorological scatterers because scattering is noncoherent in this case. The antenna measurement at $\beta = 0°$, when the transmitted wave is horizontally polarized, gives the information about amplitude and phase relations between the elements $\dot{f}_{xx}(\theta, \phi)$ and $\dot{f}_{xy}(\theta, \phi)$. The information about the elements $\dot{f}_{yx}(\theta, \phi)$ and $\dot{f}_{yy}(\theta, \phi)$ can be obtained at $\beta = 90°$. As the measurements are not coherent over long time periods, the third measurement at $\beta = 45°$ is necessary to get the correct phase difference between the measurements at $\beta = 0°$ and $\beta = 90°$.

The test transmitter was mounted at the airport tower at about 12-m height above ground. To minimize reflections from the tower, the antenna of the test transmitter was installed 1 m away from the tower walls by mounting it on a wooden bar. The radar was placed 600 m away from the tower to ensure that the test transmitter was within the far field of the radar antenna, which starts at 235-m distance. Before the measurements, the radar antenna angular position with the maximum received power was determined. At this position it is assumed that $\theta = 0°$ and $\phi = 0°$. Then the test transmitter horn was manually rotated to the position where the measured LDR was minimal. This angular position of the horn was assumed to correspond to $\beta = 0°$. The frequency of the test transmitter was set to 35.15 GHz, which corresponds to the operating frequency of the radar magnetron. To receive maximum SNR, the local oscillators of the radar were adjusted so that the center of the receiving bandwidth of the radar matches 35.15 GHz. The frequency was tuned in steps of 1 MHz and the maximum of SNR was found at a 1-MHz offset. Such an offset is within the uncertainty of the frequency synthesizers, which are mainly optimized for spectral purity and not for accurate frequency matching.

TABLE 2. Specification of used antennas.

Type	Cassegrain
Dish	Parabolic
Feed design	Center fed
No. of struts	4
Diameter (m)	1
Weight (kg)	21.5
Operation band (GHz)	35.1–35.3
Gain (dB)	49.2
Beamwidth (°)	0.6
Sidelobes (dB)	<-18
Voltage standing wave ratio (VSWR)	<1.33
Orthogonal mode transducer (OMT) coupling (dB)	-36

The scanning regime can be described as follows. The radar was scanning over the azimuth in the range from $-4°$ to $4°$ with respect to the maximum position with an angular speed $0.5° s^{-1}$. The elevation angle was changed by 0.1° after every azimuth cycle. To avoid the effects of the ground on signal propagation, the pattern measurements were performed in two steps. First, the lower half of the antenna pattern was measured. Then the antenna was rotated in both azimuth and elevation by 180° to measure the second half of the pattern in the same relative position to the ground. The overlap in elevation between these two measurements was 2°. The same procedure was done for $\beta = 45°$ and $\beta = 90°$. The $\beta = 45°$ and $\beta = 90°$ orientations were set with respect to the position with $\beta = 0°$ by using a spirit level.

The processing of the raw data with quadrature components of the received signal includes the calculation of the following parameters:

$$F_{xx}(\theta, \phi) = \frac{\langle |\dot{f}_{xx}(\theta, \phi)| \rangle}{\langle |\dot{f}_{xx}(0, 0)| \rangle}, \tag{12}$$

$$F_{xy}(\theta, \phi) = \frac{\langle |\dot{f}_{xy}(\theta, \phi)| \rangle}{\langle |\dot{f}_{xx}(0, 0)| \rangle}, \tag{13}$$

$$F_{yx}(\theta, \phi) = \frac{\langle |\dot{f}_{yx}(\theta, \phi)| \rangle}{\langle |\dot{f}_{xx}(0, 0)| \rangle}, \tag{14}$$

$$F_{yy}(\theta, \phi) = \frac{\langle |\dot{f}_{yy}(\theta, \phi)| \rangle}{\langle |\dot{f}_{xx}(0, 0)| \rangle}, \tag{15}$$

$$\alpha_1(\theta, \phi) = \langle \arg[\dot{f}_{xx}(\theta, \phi)] - \arg[\dot{f}_{xy}(\theta, \phi)] \rangle, \tag{16}$$

$$\alpha_2(\theta, \phi) = \langle \arg[\dot{f}_{yx}(\theta, \phi)] - \arg[\dot{f}_{yy}(\theta, \phi)] \rangle, \quad \text{and} \tag{17}$$

$$\alpha_3(\theta, \phi) = \langle \arg[\dot{f}_{xx}(\theta, \phi)] - \arg[\dot{f}_{yy}(\theta, \phi)] \rangle. \tag{18}$$

In Eqs. (12)–(18), F_{mn} are the normalized amplitude patterns and $\alpha_{1,2,3}$ are the phase differences between the

respective complex antenna patterns. The averaging interval was 0.2 s. The resulting apparent azimuth resolution of the antenna patterns is 0.1°. The normalized antenna patterns can be written in the matrix form

$$\mathbf{F}'(\theta,\phi) = \begin{Bmatrix} F_{xx}(\theta,\phi) & F_{yx}(\theta,\phi)e^{i[\alpha_2(\theta,\phi)-\alpha_3(\theta,\phi)]} \\ F_{xy}(\theta,\phi)e^{-i\alpha_1(\theta,\phi)} & F_{yy}(\theta,\phi)e^{-i\alpha_3(\theta,\phi)} \end{Bmatrix}. \quad (19)$$

c. *Results of antenna pattern measurements*

The results of the receiving-pattern measurements for both antennas are shown in Figs. 4–6. The measured patterns are typical for a center-fed parabolic reflector (Zrnić et al. 2010). In Fig. 4 note that the patterns of $F_{xx}(\theta, \phi)$ and $F_{yy}(\theta, \phi)$ are almost identical for both antennas. The main beams are symmetrical in the azimuth and elevation plane and their width at the half-power level is about 0.7° (Fig. 6), which is in good agreement with the technical documentation of the antennas. Visible are also two adjacent sidelobes with amplitudes of −18 and −27 dB, respectively. The second and following sidelobes have negligibly low amplitudes and do not have a significant influence on the resulting signal.

Table 3 shows the ICPR components $P_{1,2,3}$ integrated over different areas of the antenna patterns. The areas are illustrated in Fig. 7. The results indicate that the fraction of ICPR induced in the area outside of the main beam does not exceed 10% for both antennas. The combined analysis of the copolarized and cross-polarized antenna patterns shows that the polarization leakage in the center of the main beam is very low. The ratio of the cross-polarized signal to the copolarized signal yields values of about −45 and −35 dB for the good and bad antennas, respectively. It should be noted that the real values of the coupling in the beam centers can be even lower. The measured values depend not only on the quality of the horn antenna of the test transmitter but also on the accuracy of the positioning of this transmitter. Nevertheless, lower coupling values in the beam center will not change the results significantly. Such low coupling values explain the small contribution of the beam center to ICPR (zone I in Table 3). The largest contribution to ICPR for both antennas comes from zones II and III (Table 3). These zones correspond to the periphery of the main beam. Within zones II and III there are four areas with an increased leakage (the mean ratios of the cross-polarized signal to the copolarized signal are −13 and −8 dB for the good and bad antennas, respectively). These areas are formed by the struts (Chandrasekar and Keeler 1993) holding the

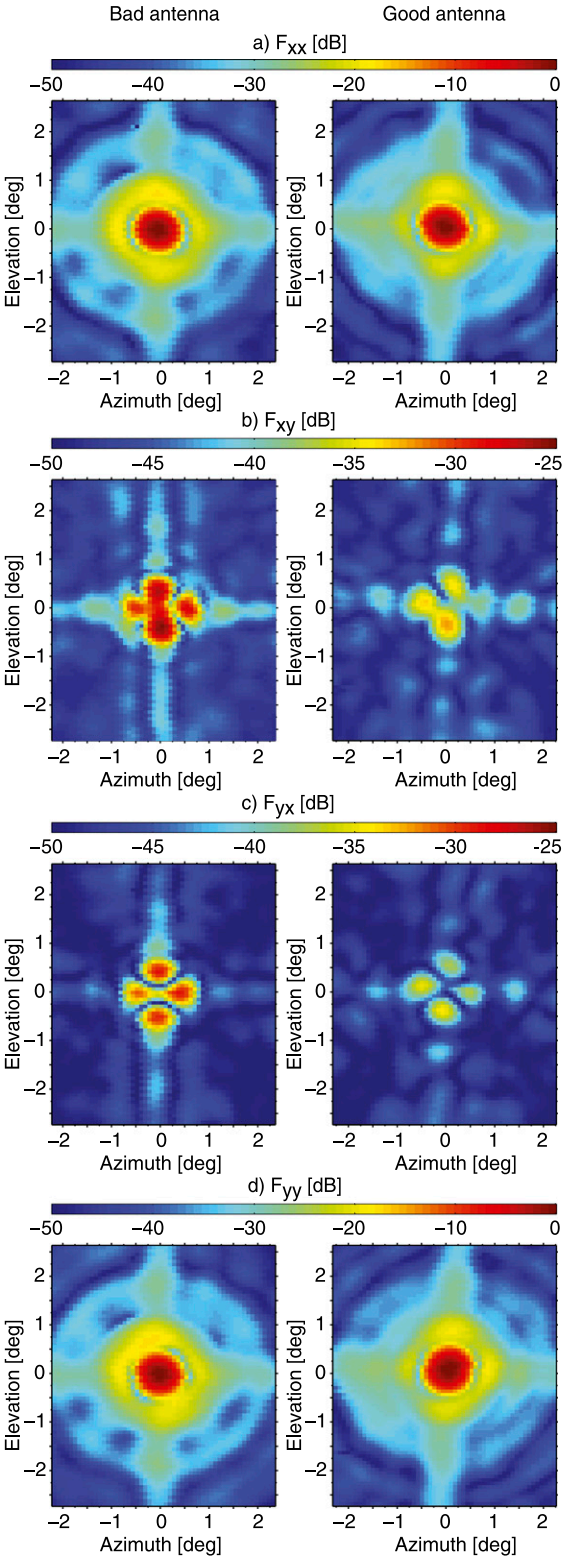

FIG. 4. Normalized amplitude antenna patterns for the (left) bad and (right) good antennas. Please note that scales for (a) and (d) differ from (b) and (c).

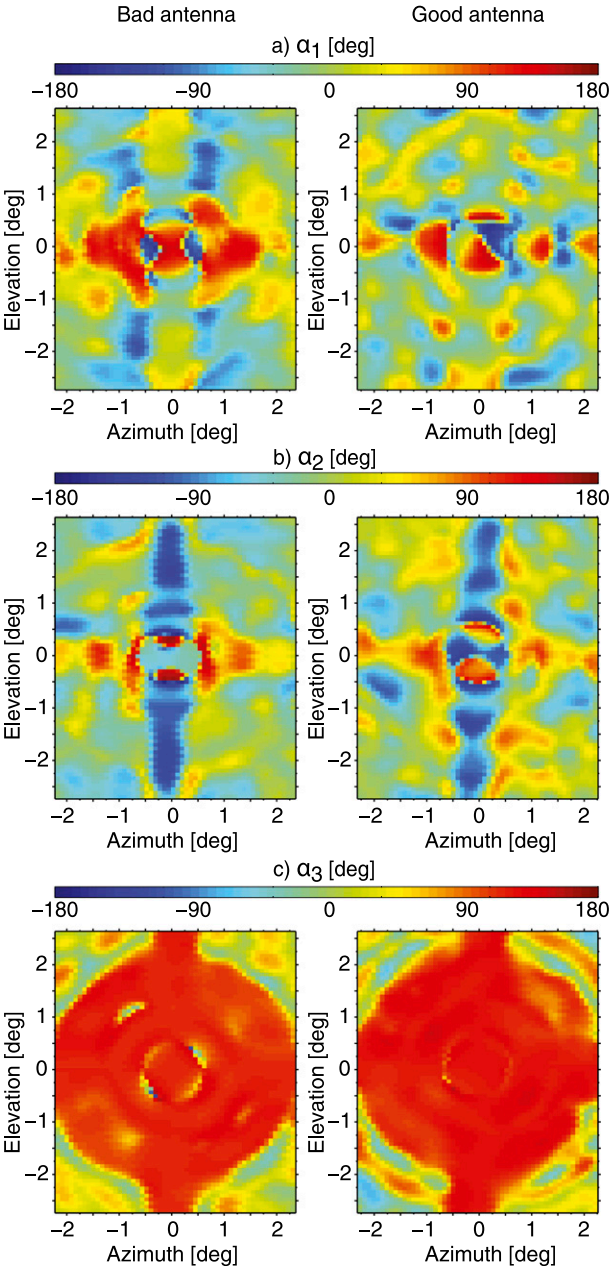

FIG. 5. Patterns of the phase differences for the (left) bad and (right) good antennas.

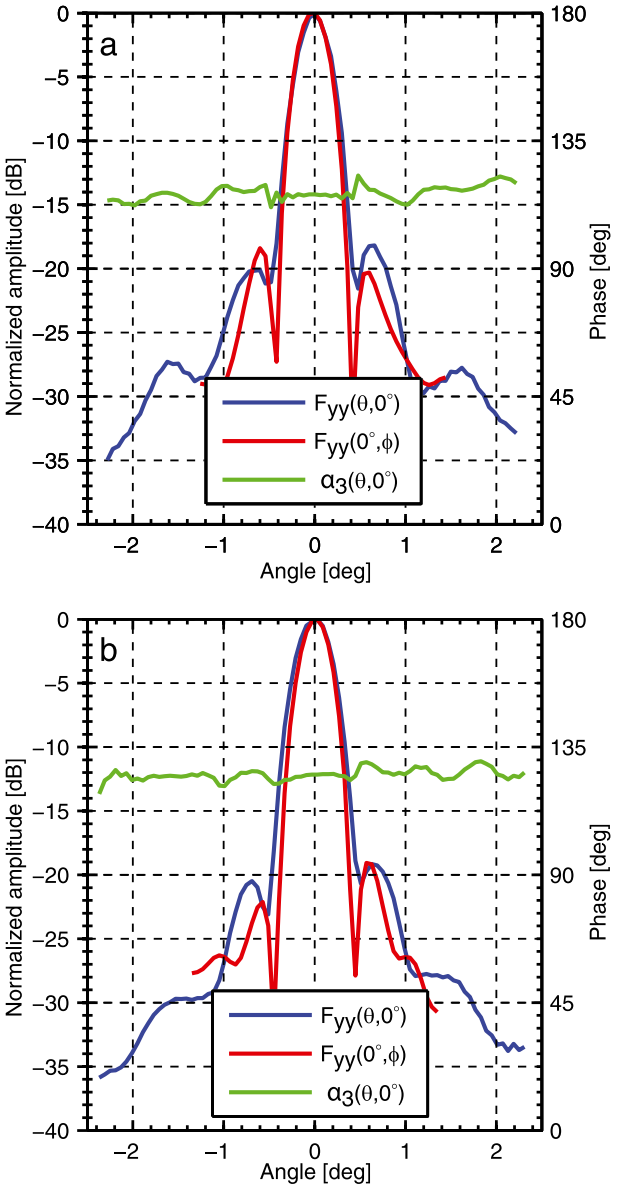

FIG. 6. Cut planes of F_{yy} over the azimuth, of F_{yy} over the elevation, and of α_3 over the azimuth for the (a) bad and (b) good antennas.

antenna subreflector (Fig. 3), which causes an increase in ICPR.

Table 3 also demonstrates the dominance of components P_1 and P_2 in ICPR for the bad antenna. The total contribution of P_3 for the bad antenna is negligibly small because negative values in the center of the main beam and positive values at the periphery of the main beam are partially canceled out. Even though in the case of the good antenna P_2 gives the largest contribution to ICPR, all the components have the same order of magnitude. Note, the P_3 contribution exceeds the P_1 contribution and cannot be neglected as in the case of the bad antenna.

From Fig. 6 it can be concluded that the phase difference $\alpha_3(\theta, \phi)$ is constant in the main beam. The standard deviation of $\alpha_3(\theta, \phi)$ within two sidelobes is 8° and 18° for the good and bad antennas, respectively. The value of $\alpha_3(\theta, \phi)$ is thus mostly defined by the different pathlengths of the co- and cross channels.

TABLE 3. Components $P_{1,2,3}$ of ICPR calculated from the measured complex antenna patterns. Values in columns I–V correspond to different integration areas (Fig. 7). All the values are given in linear units. Note that components $P_{1,2,3}$ are multiplied by 10^4.

	I	II	III	IV	V	Total
			Bad antenna			
$P_1 \times 10^4$	2.01	4.30	3.62	0.66	0.39	10.98
$P_2 \times 10^4$	5.28	10.03	4.85	0.77	0.29	21.22
$P_3 \times 10^4$	−4.45	−2.62	5.71	0.86	0.46	−0.04
$\sum_{i=1}^{3} P_i \times 10^4$	2.84	11.71	14.18	2.30	1.14	32.17
			Good antenna			
$P_1 \times 10^4$	0.10	0.44	0.48	0.09	0.04	1.16
$P_2 \times 10^4$	0.45	1.70	1.18	0.19	0.08	3.60
$P_3 \times 10^4$	−0.13	0.73	0.93	0.10	0.04	1.66
$\sum_{i=1}^{3} P_i \times 10^4$	0.42	2.87	2.58	0.38	0.16	6.42

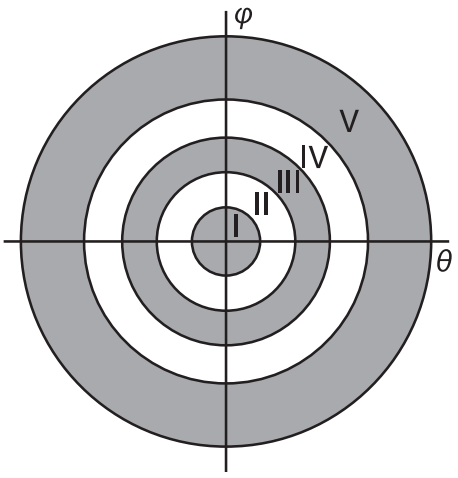

FIG. 7. Integration areas. The areas I–V have outer radii of 0.2°, 0.4°, 0.6°, 0.8°, and 2.5°, respectively. All the radii are with respect to the position $\theta = 0°$ and $\phi = 0°$.

The evaluation of $\alpha_{1,2}(\theta, \phi)$ shows that the phase difference between the cross-polarized and copolarized signals is not constant over the whole antenna pattern, especially in zones II and III, which produce up to 80% of the polarization leakage.

Using the measured antenna patterns, ICPR can be calculated from Eqs. (5) and (19). These calculations yield ICPR values of −24.9 and −31.9 dB for the bad and good antennas, respectively. As shown in section 2a, the corresponding ICPR values measured with a vertically aligned beam in light-rain conditions were about −25 and −31 dB, respectively. Thus, we can conclude that there is a relatively good agreement between the calculated and measured ICPR values.

To assess the impact of the phase differences on the estimate of ICPR, we compared this estimate with the upper bound of ICPR calculated only from amplitude antenna patterns (Chandrasekar and Keeler 1993):

$$\mathrm{ICPR}_{\mathrm{ub}} = \frac{\int [F_{xx}(\theta,\phi)F_{xy}(\theta,\phi) + F_{yx}(\theta,\phi)F_{yy}(\theta,\phi)]^2 \, d\Omega}{\int [F_{xx}(\theta,\phi)^2 - F_{yx}(\theta,\phi)^2]^2 \, d\Omega}. \tag{20}$$

Calculated values of $\mathrm{ICPR}_{\mathrm{ub}}$ are −22.3 and −30.8 dB for the bad and good antenna, respectively. The $\mathrm{ICPR}_{\mathrm{ub}}$ value of the bad antenna is about 2.5 dB higher than the ICPR value estimated in light rain and the one calculated from the antenna patterns. The $\mathrm{ICPR}_{\mathrm{ub}}$ value of the good antenna is 0.2 dB and 1.1 dB higher than the ICPR value estimated in light rain and the one calculated from the antenna patterns, respectively.

Analysis of Table 4 data shows that the components of the bias in the correlation coefficient are mainly formed in the main antenna beam (zones I–III). Values of ρ_b calculated from the antenna patterns are 0.4 and 0.1 for the good and bad antenna, respectively. Those measured in light rain are 0.37 and 0.17, respectively.

The values of ICPR and ρ_b allow for an estimation of the degree of polarization (Galletti et al. 2012):

$$\mu = \left[1 - \frac{4\mathrm{ICPR}}{(1+\mathrm{ICPR})^2}(1-\rho_b^2)\right]^{1/2}. \tag{21}$$

The degree of polarization in the case of isotropic scatterers should be strictly equal to 1; that is, the received wave should be fully polarized (Galletti et al. 2012). Nevertheless, μ calculated for isotropic particles using the antenna patterns are 0.9946 and 0.9987 for the bad and good antenna, respectively. This indicates that the received wave has a nonpolarized component that is produced by the antenna system.

In the next section we present an approach for the correction of polarimetric variables obtained in

TABLE 4. Components $R_{1,2}$ of ρ_b calculated from the measured complex antenna patterns. Integration areas are the same as in Table 3. Note that components $R_{1,2}$ are multiplied by 10^2.

	I	II	III	IV	V	Total
			Bad antenna			
$R_1 \times 10^2$	4.26	10.04	4.20	0.23	−0.15	18.58
$R_2 \times 10^2$	−16.77	−18.06	−1.43	0.36	0.11	−35.81
			Good antenna			
$R_1 \times 10^2$	1.80	3.89	3.50	0.22	−0.12	9.28
$R_2 \times 10^2$	6.91	−1.46	−6.65	0.03	0.07	−1.09

the LDR mode, applying a decomposition of the coherency matrix into nonpolarized and fully polarized parts.

3. Correction of the LDR measurements

Electromagnetic waves with $0 < \mu < 1$ are denoted as partly polarized waves. The polarization state of a partly polarized wave can be characterized statistically by the 2×2 coherency matrix (Kanareykin et al. 1966, 1968; Born and Wolf 1975):

$$\mathbf{J} = \begin{pmatrix} J_{11} & \dot{J}_{12} \\ \dot{J}_{21} & J_{22} \end{pmatrix}. \tag{22}$$

The elements of the coherency matrix **J** can be calculated as follows (McCormick and Hendry 1975):

$$J_{11} = \langle \dot{E}_x \dot{E}_x^* \rangle, \tag{23}$$

$$\dot{J}_{12} = \langle \dot{E}_x \dot{E}_y^* \rangle, \tag{24}$$

$$\dot{J}_{21} = \langle \dot{E}_y \dot{E}_x^* \rangle, \quad \text{and} \tag{25}$$

$$J_{22} = \langle \dot{E}_y \dot{E}_y^* \rangle, \tag{26}$$

where $\dot{E}_x$ and $\dot{E}_y$ are complex amplitudes of the received signals in the horizontal and vertical polarization channels, respectively; and the angle brackets ($\langle\ \rangle$) mean averaging over time. The complex amplitudes for every received pulse are expressed using the I and Q components measured by the radar:

$$\dot{E}_x = I_x + iQ_x \quad \text{and} \tag{27}$$

$$\dot{E}_y = I_y + iQ_y. \tag{28}$$

The elements J_{11} and J_{22} are real quantities describing the received powers in the co- and cross channels, respectively. The complex element $\dot{J}_{12}$ defines the covariance between the signals in the co- and cross channels. It is necessary to note that $\dot{J}_{12} = \dot{J}_{21}^*$. In terms of the coherency matrix elements, LDR can be written in the following form:

$$\mathrm{LDR} = \frac{J_{22}}{J_{11}}. \tag{29}$$

It should be emphasized that Eq. (29) is only valid when the coherency matrix is specified in the polarimetric basis formed by horizontal and vertical unit vectors.

The link between the coherency matrix elements for the case of scattering from distributed isotropic particles and corresponding antenna patterns can be found in Chandrasekar and Keeler (1993). It is shown in Kanareykin et al. (1966) that the probability density function of the phase shift between the orthogonal components is defined by two parameters: $\gamma = \arg(\dot{J}_{12})$, which specifies the mean value of $\Delta\Phi$; and the correlation coefficient:

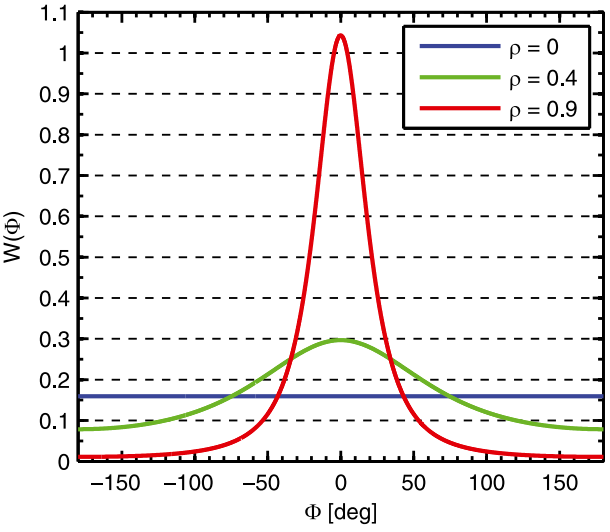

FIG. 8. Centralized probability density function $W(\Phi)$, where $\Phi = \Delta\Phi - \gamma$. Adopted from Kanareykin et al. (1966).

$$\rho = |\dot{J}_{12}| \Big/ \sqrt{J_{11} J_{22}}, \tag{30}$$

which defines the width of $W(\Delta\Phi)$ (Fig. 8).

The coherency matrix of a partly polarized wave can be represented as the sum of two components (Kanareykin et al. 1966; Born and Wolf 1975):

$$\mathbf{J} = A\mathbf{I} + \begin{pmatrix} B & \dot{D} \\ \dot{D}^* & C \end{pmatrix} \tag{31}$$

with the condition

$$BC - |\dot{D}|^2 = 0, \tag{32}$$

where **I** is a 2×2 unit matrix. Terms A, B, C, and $\dot{D}$ can be calculated with the following equations (Kanareykin et al. 1966; Born and Wolf 1975):

$$A = \frac{1}{2}[\mathrm{Sp}\mathbf{J} - (\mathrm{Sp}^2\mathbf{J} - 4\mathrm{det}\mathbf{J})^{1/2}], \tag{33}$$

$$B = \frac{1}{2}[J_{11} - J_{22} + (\mathrm{Sp}^2\mathbf{J} - 4\mathrm{det}\mathbf{J})^{1/2}], \tag{34}$$

$$C = \frac{1}{2}[J_{22} - J_{11} + (\mathrm{Sp}^2\mathbf{J} - 4\mathrm{det}\mathbf{J})^{1/2}], \tag{35}$$

$$\dot{D} = \dot{J}_{12}. \tag{36}$$

Here Sp is the matrix trace and det is the matrix determinant.

In Eq. (31) the first and second components describe the nonpolarized and fully polarized parts of the electromagnetic wave, respectively; that is, the received electromagnetic wave can be presented as a sum of nonpolarized and fully polarized waves. The nonpolarized part does not have a major polarization state, and the phase shift between its orthogonal components is uniformly distributed, so that the co-cross-polar correlation coefficient of the nonpolarized wave is 0. The fully polarized part is characterized by a constant polarization state. The correlation coefficient of the fully polarized wave is 1.

In the case of vertical sensing of hydrometeors consisting of drizzle or light rain, the scattering volume can be assumed to be isotropic. Under this condition the parameters A_i, B_i, C_i (we use the index i for marking the case of isotropic scattering only) can be calculated from the I/Q measurements using Eqs. (22)–(28) and (33)–(35). Further, we neglect the leakage from the cross channel into the cochannel and introduce the normalized parameters:

$$A_i' = \frac{A_i}{B_i} \quad \text{and} \tag{37}$$

$$C_i' = \frac{C_i}{B_i}. \tag{38}$$

The parameter A_i' describes the power of the noncoherent leakage from the cochannel into the cross channel that is formed by the antenna system. The parameter C_i' describes the power of the coherent leakage that is produced by the antenna system. As isotropic particles do not change the polarization state of the scattered wave, the polarimetric properties of the received wave are defined by the antenna system of the radar. Parameters A_i' and C_i' are stable in time under the assumption that the radar characteristics are constant. For radar 1 equipped with the bad antenna, mean values of A_i' and C_i' found from vertical measurements in light rain using Eqs. (33)–(35) are −25.3 and −32.9 dB, respectively. Those for radar 2 with the good antenna are −30.9 and −47.6 dB, respectively.

The LDR for isotropic scatterers can be presented in terms of the decomposed coherency matrix elements:

$$\mathrm{LDR}_i = \mathrm{ICPR} = \frac{A_i' + C_i'}{A_i' + 1}. \tag{39}$$

As shown previously, the ICPR of a given radar system can be either calculated using measurements of complex antenna patterns and Eqs. (5) and (19), or it can be measured in drizzle or light rain as shown in section 2a. Measurements in drizzle were used previously to determine ICPR for cloud radars of the National Oceanic and Atmospheric Administration (NOAA) and the U.S. Department of Energy (DOE) as described in Matrosov et al. (2001, 2012).

For anisotropic scatterers the fully polarized and nonpolarized parts of the backscatter signals depend not only on the radar hardware properties but also on the scattering properties of the scatterers. As it was mentioned above, ρ, which also influences the fully polarized and nonpolarized fractions of the received wave (Galletti et al. 2012), depends on shape, orientation, and dielectric properties of the scatterers.

Hydrometeors are usually assumed to have a linear eigen-polarization basis (Bringi and Chandrasekar 2001). The polarimetric properties of backscatter signals produced by such scatterers can be decomposed into isotropic and anisotropic parts (Tatarinov and Tatarinov 2011). Taking this into account, the expressions for the elements A and C of the coherency matrix can be rewritten in the following form:

$$A = A_i + A_a \quad \text{and} \tag{40}$$

$$C = C_i + C_a, \tag{41}$$

where A_a and C_a are the nonpolarized and fully polarized components of the received signals produced by anisotropic scattering in the cross channel, respectively. As it was shown previously, the isotropic part of the signal in the cross channel is defined by the radar hardware. Using Eqs. (30)–(32), (40), and (41), LDR and ρ can be presented as follows:

$$\mathrm{LDR} = \frac{A_i + A_a + C_i + C_a}{A_i + A_a + B} \quad \text{and} \tag{42}$$

$$\rho = \frac{\sqrt{B(C_i + C_a)}}{\sqrt{(A_i + A_a + B)(A_i + A_a + C_i + C_a)}}. \tag{43}$$

The corrected values of A, B, and C—that is, the values that would be observed in case of an ideal radar—can be written as

$$A_{\mathrm{cor}} = \begin{cases} A - \langle A_i' \rangle B, & \text{if} \quad A/B > \langle A_i' \rangle + 3\sigma(A_i') \\ 0, & \text{otherwise} \end{cases}, \tag{44}$$

$$B_{\mathrm{cor}} = B(1 + \langle A_i' \rangle + \langle C_i' \rangle) \quad \text{and} \tag{45}$$

$$C_{\mathrm{cor}} = \begin{cases} C - \langle C_i' \rangle B, & \text{if} \quad C/B > \langle C_i' \rangle + 3\sigma(C_i') \\ 0, & \text{otherwise} \end{cases}. \tag{46}$$

In Eqs. (44) and (46) σ is the standard deviation. The averages and standard deviations in Eqs. (44)–(46) are taken from the regions where rain or drizzle is observed.

The conditions introduced in Eqs. (44) and (46) are necessary to reduce the errors caused by noise. Then, the corrected values of LDR and ρ can be obtained by using Eqs. (44)–(46):

$$\mathrm{LDR}_{\mathrm{cor}} = \frac{A_{\mathrm{cor}} + C_{\mathrm{cor}}}{A_{\mathrm{cor}} + B_{\mathrm{cor}}} \quad \text{and} \tag{47}$$

$$\rho_{\mathrm{cor}} = \frac{\sqrt{B_{\mathrm{cor}} C_{\mathrm{cor}}}}{\sqrt{(A_{\mathrm{cor}} + B_{\mathrm{cor}})(A_{\mathrm{cor}} + C_{\mathrm{cor}})}}. \tag{48}$$

For isotropic particles both A_{cor} and C_{cor} are equal to 0. Thus, Eq. (48) contains the indeterminate form 0/0 and the value of ρ_{cor} is undefined (Galletti et al. 2012). In this case we replace the value of ρ_{cor} by the limit:

$$\lim_{J_{22}\to 0} \frac{|\dot{J}_{12}|}{\sqrt{J_{11} J_{22}}}. \tag{49}$$

In the case of reflection symmetry (e.g., randomly oriented particles) $|\dot{J}_{12}| = 0$ (Nghiem et al. 1992; Ryzhkov 2001). Under this condition the limit in Eq. (49) becomes 0.

It is assumed that the cloud particles in a low-turbulence environment are mostly oriented with their major dimensions in the horizontal plane (Matrosov et al. 2012). In this case, for the LDR mode, A and C are several orders of magnitude smaller than B, so $A_i' \ll 1$ and $C_i' \ll 1$, and Eqs. (47) and (48) can be simplified as follows:

$$\mathrm{LDR}_{\mathrm{cor}} \approx \mathrm{LDR} - \mathrm{ICPR} \quad \text{and} \tag{50}$$

$$\rho_{\mathrm{cor}} \approx \sqrt{\frac{C - C_i' B}{B(\mathrm{LDR} - \mathrm{ICPR})}}. \tag{51}$$

The result similar to the Eq. (50) was previously given by Ryzhkov et al. (2002).

As an example, the results of the LDR correction for the vertical profiles shown in Fig. 2 are depicted in Figs. 9 and 10. The minimum value of corrected LDR was limited to −40 dB to make the figures more illustrative. It can be seen in Fig. 9 that the correction procedure lowered LDR values in the rain regions by more than 7 dB for both radars. The correction results are also noticeable in the ice region that was present above about 1.5-km height. Observed and corrected LDR values for the melting layers are approximately the same. Even though the difference between the corrected LDR of radar 1 and radar 2 can reach several decibels, the values are on average similar (Fig. 10). The data scatter in Fig. 10, which generally increases with decreasing LDR, provides a measure for uncertainty in the LDR correction. For very low LDR (<−35 dB), measurement noise

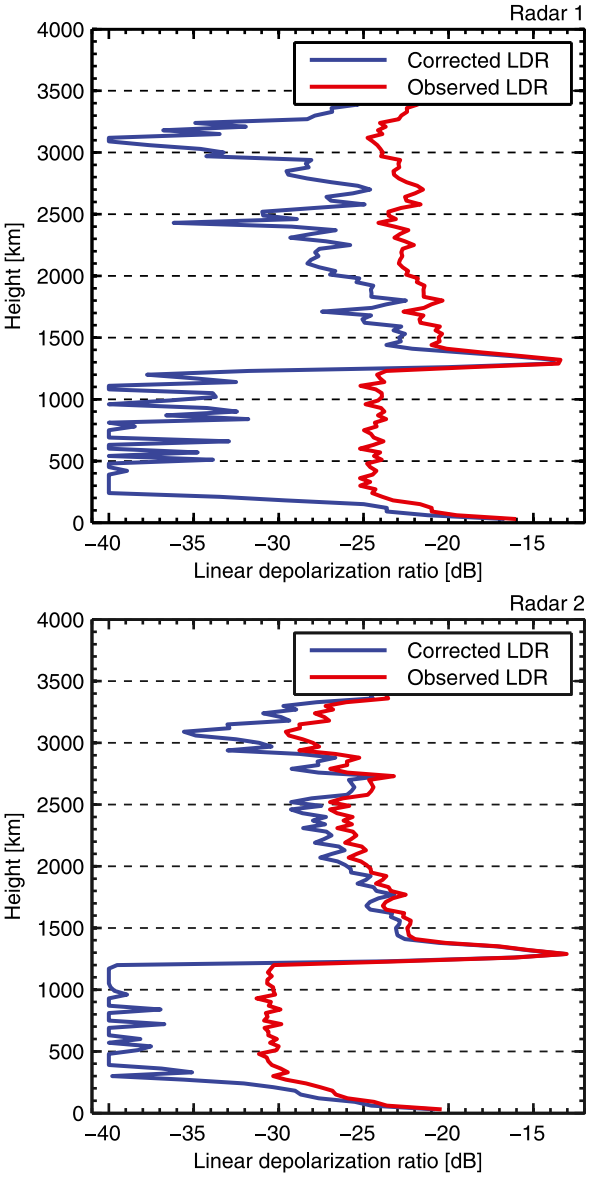

FIG. 9. Vertical profiles of LDR for radars 1 and 2 for the same case as in Fig. 2.

is already playing a major role. For such low values we consider differences in corrected LDR to be mostly due to noise and correction uncertainties. The mean behavior of the corrected LDR profiles above the melting layer is similar for both radars. The differences in the variability (i.e., deviations from the mean) are believed to be mostly due to correction uncertainties and measurement noise. The height–time cross sections of the corrected LDR are presented in Fig. 11.

The results of the correction of the correlation coefficient are presented in Fig. 11 as well. The data for this figure were acquired with the vertically pointed radars at

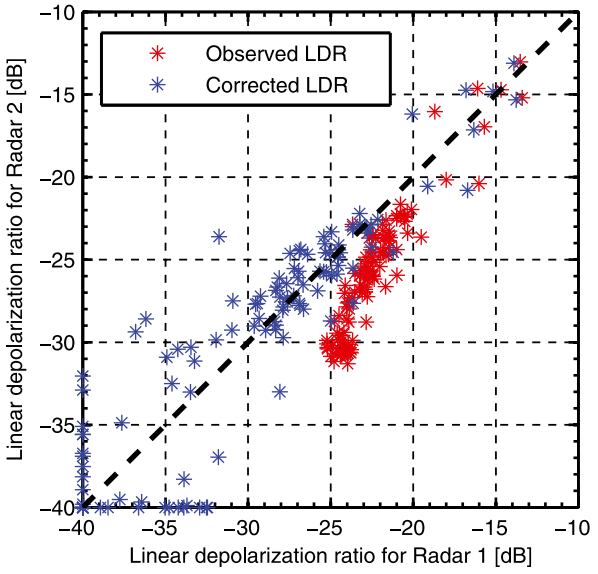

FIG. 10. Scatterplot of observed (red dots) and corrected (blue dots) values of LDR for radars 1 and 2 for the same case as in Fig. 9.

the METEK site. In Figs. 11a and 11b the height–time cross sections of the observed (i.e., not corrected) ρ for radar 1 and radar 2, respectively, are presented. The melting layer can be seen at 1.5-km height. Particles in this layer have strongly nonspherical shapes and their orientation is random in the polarization plane. Therefore, the observed values of the correlation coefficient for the melting layer are close to 0 because the nonpolarized component of the received signals is mostly defined by the scattering characteristics of the particles and not by the radar hardware properties. Light rain was observed below the melting layer. The values of the observed ρ for radar 1 are in the range of 0.3–0.4, while for radar 2 those values are about 0.1–0.2. The values of observed ρ for the rain are mostly defined by the radar hardware, and they are different for every radar. Above the melting layer, the radars observed ice crystals. Some areas with decreased values of observed ρ can be clearly seen in Fig. 11a. Ice particles in these areas are not isotropic. For instance, this can occur when some columnar-shaped particles are present or nonspherical particles have a wide distribution in canting angle (Matrosov 1991). Both cases lead to increased values of LDR that can be apparently seen in Fig. 1.

In Figs. 11c and 11d the height–time plots of the corrected correlation coefficient ρ_{cor} are shown. For the whole cloud system ρ_{cor} is close to 0. This indicates that particles are either isotropic or nonspherical with random orientation in the polarization plane (Ryzhkov

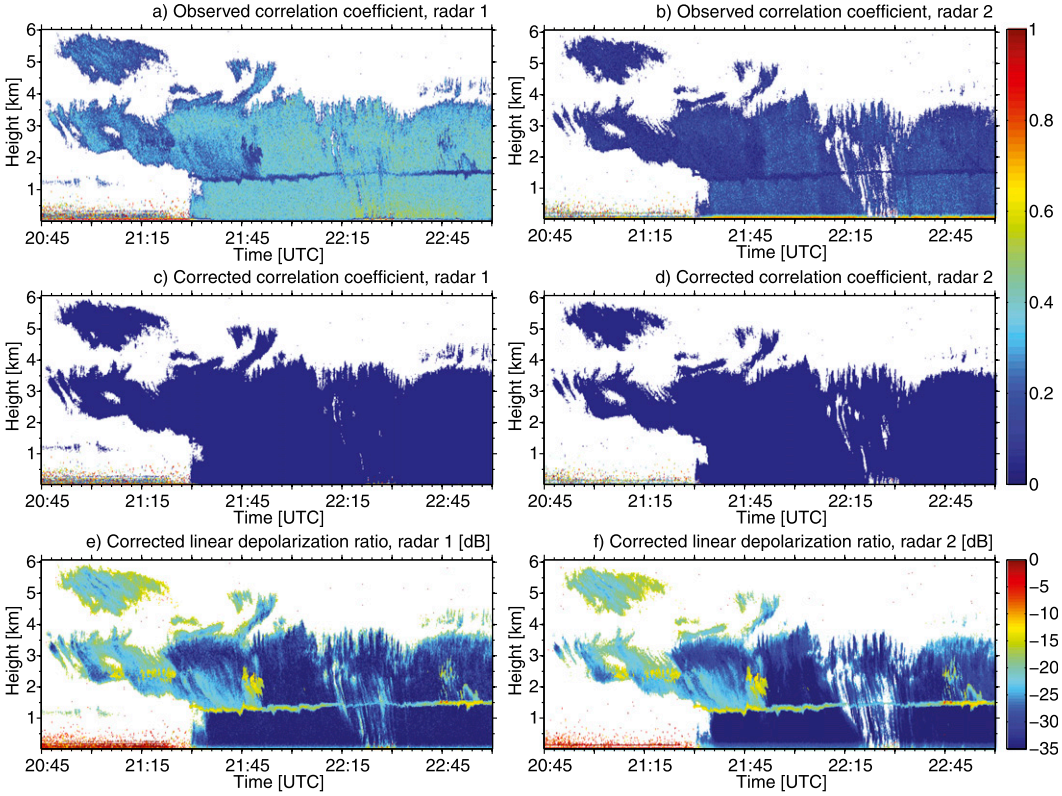

FIG. 11. Observed correlation coefficient for (a) radar 1 and (b) radar 2, corrected correlation coefficient for (c) radar 1 and (d) radar 2, and corrected LDR for (e) radar 1 and (f) radar 2 for the same case as in Fig. 1.

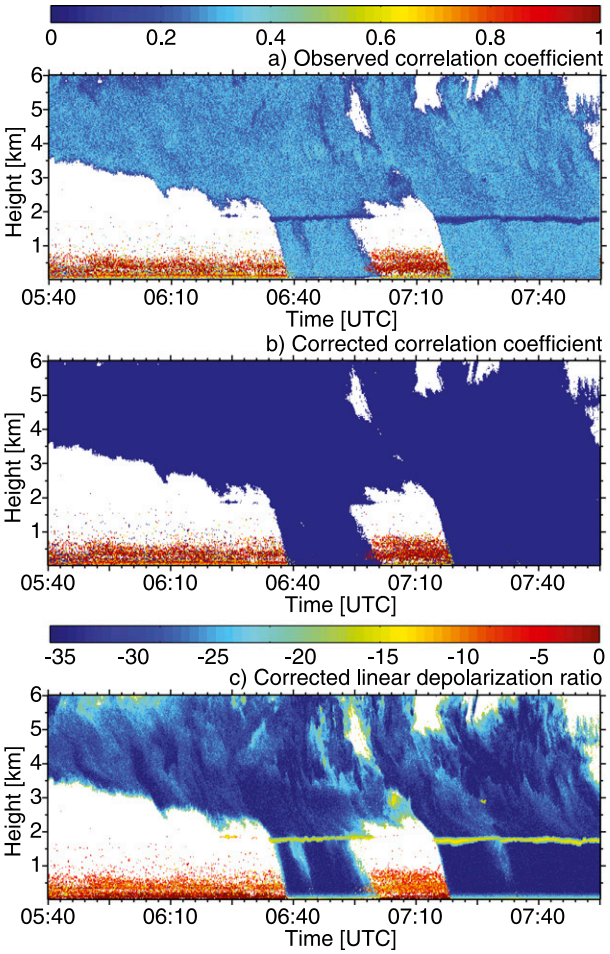

FIG. 12. (a) Observed and (b) corrected correlation coefficient, and (c) corrected LDR for the measurement taken with radar 1 at Elmshorn on 12 Sep 2013.

2001; Ryzhkov et al. 2002) such as particles in the melting layer.

Figure 12 shows height–time cross sections of observed and corrected correlation coefficients and corrected LDR for a measurement taken at the METEK site in Elmshorn on 12 September 2013. The melting layer, characterized by low values of both observed and corrected correlation coefficients and LDR of −15 dB, was observed at about 1.7-km height. Above the melting layer, falling ice particles were observed, while below the melting layer light rain occurred. The echoes with high values of observed ρ and LDR near the ground below 800 m correspond to insects. It can be seen that for insects, observed and corrected correlation coefficients do not differ significantly. This indicates that the co- and cross-polarized components of the received signal are highly correlated either due to the preferred orientation of insects, which is consistent with other observations (Zrnić and Ryzhkov 1998), or the low concentration of insects in the resolution volume (or both). It is known that insects can be considered as point scatterers that produce strong depolarization (Martner and Moran 2001). In this case the antenna system produces the narrow distribution of the phase difference between the co- and cross-channel signals (Fig. 5c) that leads to the high values of ρ. This fact can be used for the separation of insects (point scatterers) and clouds (distributed scatterers).

4. Summary and conclusions

Cloud radars used in atmospheric studies are often operated in the LDR mode when the horizontally and vertically polarized components of received echoes are measured, while only horizontally polarized pulses are transmitted. Often the phase relations between these components are also measured in addition to the Doppler spectrum moments. The polarimetric variables, which are typically available from this measurement mode, are the linear depolarization ratio and the correlation coefficient ρ between the copolar and cross-polar components of returned signals.

Radar hardware (e.g., antennas) affects the quality of polarimetric variables and, as a result, the observed LDR and ρ can be biased. Polarization leakage between receiving channels results in elevated LDR values. These biases are usually small compared to values from highly anisotropic scatterers and can be significant for isotropic scatterers. Because of the polarization leakage, radar measurements of the depolarization ratio are limited by a minimal LDR value (i.e., ICPR). Biases are also present in the correlation coefficient measurements. The ICPR and the bias in ρ depend on the quality of the antenna system and thus are specific for a particular radar. These values can be estimated using the results of high-resolution measurements of complex antenna patterns.

Measurements of the antenna patterns were performed for the antenna systems of two METEK Ka-band cloud radars, one with a good polarimetric isolation and the other with a pure polarization isolation. It was shown that up to 80% of polarization leakage is produced by the struts holding the antenna subreflector. Using results of the antenna pattern measurements, ICPR and the bias in ρ were calculated. The obtained values of ICPR (approximately −25 and −32 dB for the bad and good antennas, respectively) were in good agreement with independent ICPR estimates found from vertically pointing measurements in light rain. The ρ biases were found to be about 0.4 and 0.1 for the two antennas, respectively. Estimates of the differences between ICPR values

calculated using complex antenna patterns and the upper ICPR bounds computed using the amplitude patterns only were found not to exceed 2.5 dB.

A coherency matrix formalism was used to develop an algorithm to correct the observed LDR and ρ in order to estimate these polarimetric variables for a hypothetical case of almost ideal hardware. We recommend using the vertical measurements in light rain or drizzle for the estimation of ICPR and the elements of the coherency matrix for subsequent corrections of polarimetric variables. Introducing these corrections allows for a more meaningful analysis of measurements and comparability of LDR and ρ measured by different radars with antenna systems of different qualities, thus emphasizing hydrometeor influences and minimizing hardware influences on these polarimetric variables. Since LDR and ρ depend on scatterer orientations (e.g., Ryzhkov 2001), measurements of these polarimetric variables can potentially be used for retrieving hydrometeor orientation information. The use of corrected LDR and ρ will be essential for such retrievals.

The correction algorithm was evaluated using measurements of precipitating cloud systems. The intercomparison results from two collocated MIRA-35 cloud radars indicated that the correction uncertainty for LDR was about 3 dB for intrinsic LDR values in a typical range from −30 to −10 dB. The results of applying the correction algorithm to the correlation coefficient show that for volumes filled with isotropic scatterers, values of the correlation coefficient were 0 as expected from theoretical considerations.

The correction of LDR according to Eq. (50) does not require any specific data and can be implemented in operational cloud radars. The operational correction of ρ is possible when I/Q data or coherency matrix measurements are available.

Acknowledgments. The research leading to these results has been performed in the framework of Initial Training for Atmospheric Remote Sensing (ITaRS) and has received funding from the European Union's Seventh Framework Programme (Grant Agreement 289923).

REFERENCES

Born, M., and E. Wolf, 1975: *Principles of Optics: Electromagnetic Theory of Propagation, Interference and Diffraction of Light.* 5th ed. Pergamon Press, 836 pp.

Bringi, V. N., and V. Chandrasekar, 2001: *Polarimetric Doppler Weather Radar.* Cambridge University Press, 664 pp.

Chandrasekar, V., and R. J. Keeler, 1993: Antenna pattern analysis and measurements for multiparameter radars. *J. Atmos. Oceanic Technol.*, **10**, 674–683, doi:10.1175/1520-0426(1993)010<0674:APAAMF>2.0.CO;2.

Di Girolamo, P., D. Summa, M. Cacciani, E. G. Norton, G. Peters, and Y. Dufournet, 2012: Lidar and radar measurements of the melting layer: Observations of dark and bright band phenomena. *Atmos. Chem. Phys.*, **12**, 4143–4157, doi:10.5194/acp-12-4143-2012.

Donovan, D. P., and A. C. A. P. van Lammeren, 2001: Cloud effective particle size and water content profile retrievals using combined lidar and radar observations: 1. Theory and examples. *J. Geophys. Res.*, **106**, 27 425–27 448, doi:10.1029/2001JD900243.

Eloranta, E., T. Uttal, and M. Shupe, 2007: Cloud particle size measurements in Arctic clouds using lidar and radar data. *IEEE International Geoscience and Remote Sensing Symposium: Sensing and Understanding Our Planet (IGARSS 2007)*, IEEE, 2265–2267, doi:10.1109/IGARSS.2007.4423292.

Frech, M., B. Lange, T. Mammen, J. Seltmann, C. Morehead, and J. Rowan, 2013: Influence of a radome on antenna performance. *J. Atmos. Oceanic Technol.*, **30**, 313–324, doi:10.1175/JTECH-D-12-00033.1.

Galletti, M., 2013: Atmospheric radar. International Patent WO/2013/192308A1, filed 19 June 2013, and published 27 December 2013.

——, D. S. Zrnić, V. M. Melnikov, and R. J. Doviak, 2012: Degree of polarization at horizontal transmit: Theory and applications for weather radar. *IEEE Trans. Geosci. Remote Sens.*, **50**, 1291–1301, doi:10.1109/TGRS.2011.2167516.

——, ——, F. Gekat, and P. Goelz, 2014: Eigenvalue signal processing for weather radar polarimetry: Removing the bias induced by antenna coherent cross-channel coupling. *IEEE Trans. Geosci. Remote Sens.*, **52**, 7695–7707, doi:10.1109/TGRS.2014.2316821.

Görsdorf, U., V. Lehmann, M. Bauer-Pfundstein, G. Peters, D. Vavriv, V. Vinogradov, and V. Volkov, 2015: A 35-GHz polarimetric Doppler radar for long-term observations of cloud parameters—Description of system and data processing. *J. Atmos. Oceanic Technol.*, **32**, 675–690, doi:10.1175/JTECH-D-14-00066.1.

Illingworth, A. J., and Coauthors, 2007: Cloudnet: Continuous evaluation of cloud profiles in seven operational model using ground-based observations. *Bull. Amer. Meteor. Soc.*, **88**, 883–898, doi:10.1175/BAMS-88-6-883.

Kanareykin, D. B., N. F. Pavlov, and V. A. Potechin, 1966: *Polarization of Radar Signals* (in Russian). Soviet Radio Press, 440 pp.

——, V. A. Potechin, and I. F. Shishkin, 1968: *Marine Radio Polarimetry* (in Russian). Sudostroenie, 328 pp.

Kollias, P., E. E. Clothiaux, M. A. Miller, B. A. Albrecht, G. L. Stephens, and T. P. Ackerman, 2007: Millimeter-wavelength radars: New frontier in atmospheric cloud and precipitation research. *Bull. Amer. Meteor. Soc.*, **88**, 1608–1624, doi:10.1175/BAMS-88-10-1608.

Lohmeier, S. P., S. M. Sekelsky, J. M. Firda, G. A. Sadowy, and R. E. McIntosh, 1997: Classification of particles in stratiform clouds using the 33 and 95 GHz polarimetric cloud profiling radar system (CPRS). *IEEE Trans. Geosci. Remote Sens.*, **35**, 256–270, doi:10.1109/36.563264.

Martner, B. E., and K. P. Moran, 2001: Using cloud radar polarization measurements to evaluate stratus cloud and insect echoes. *J. Geophys. Res.*, **106**, 4891–4897, doi:10.1029/2000JD900623.

Matrosov, S. Y., 1991: Theoretical study of radar polarization parameters obtained from cirrus clouds. *J. Atmos. Sci.*, **48**, 1062–1070, doi:10.1175/1520-0469(1991)048<1062:TSORPP>2.0.CO;2.

——, 2015: Evaluations of the spheroidal particle model for describing cloud radar depolarization ratios of ice hydrometeors. *J. Atmos. Oceanic Technol.*, **32**, 865–879, doi:10.1175/JTECH-D-14-00115.1.

——, and R. A. Kropfli, 1993: Cirrus cloud studies with elliptically polarized Ka-band radar signals: A suggested approach. *J. Atmos. Oceanic Technol.*, **10**, 684–692, doi:10.1175/1520-0426(1993)010<0684:CCSWEP>2.0.CO;2.

——, R. F. Reinking, R. A. Kropfli, B. E. Martner, and B. W. Bartram, 2001: On the use of radar depolarization ratios for estimating shapes of ice hydrometeors in winter clouds. *J. Appl. Meteor.*, **40**, 479–490, doi:10.1175/1520-0450(2001)040<0479:OTUORD>2.0.CO;2.

——, G. G. Mace, R. Marchand, M. D. Shupe, A. G. Hallar, and I. B. McCubbin, 2012: Observations of ice crystal habits with a scanning polarimetric W-band radar at slant linear depolarization ratio mode. *J. Atmos. Oceanic Technol.*, **29**, 989–1008, doi:10.1175/JTECH-D-11-00131.1.

McCormick, G. C., and A. Hendry, 1975: Principles for the radar determination of the polarization properties of precipitation. *Radio Sci.*, **10**, 421–434, doi:10.1029/RS010i004p00421.

Mudukutore, A., V. Chandrasekar, and E. A. Mueller, 1995: The differential phase pattern of the CSU CHILL radar antenna. *J. Atmos. Oceanic Technol.*, **12**, 1120, doi:10.1175/1520-0426(1995)012<1120:TDPPOT>2.0.CO;2.

Nghiem, S. V., S. H. Yueh, R. Kwok, and F. K. Li, 1992: Symmetry properties in polarimetric remote sensing. *Radio Sci.*, **27**, 693–711, doi:10.1029/92RS01230.

Park, H., A. V. Ryzhkov, D. S. Zrnić, and K.-E. Kim, 2009: The hydrometeor classification algorithm for the polarimetric WSR-88D: Description and application to an MCS. *Wea. Forecasting*, **24**, 730, doi:10.1175/2008WAF2222205.1.

Rambukkange, M. P., J. Verlinde, E. W. Eloranta, C. J. Flynn, and E. E. Clothiaux, 2011: Using Doppler spectra to separate hydrometeor populations and analyze ice precipitation in multilayered mixed-phase clouds. *IEEE Geosci. Remote Sens. Lett.*, **8**, 108–112, doi:10.1109/LGRS.2010.2052781.

Ryzhkov, A. V., 2001: Interpretation of polarimetric radar covariance matrix for meteorological scatterers: Theoretical analysis. *J. Atmos. Oceanic Technol.*, **18**, 315–328, doi:10.1175/1520-0426(2001)018<0315:IOPRCM>2.0.CO;2.

——, D. S. Zrnić, J. C. Hubbert, V. N. Bringi, J. Vivekanandan, and E. A. Brandes, 2002: Polarimetric radar observations and interpretation of co-cross-polar correlation coefficients. *J. Atmos. Oceanic Technol.*, **19**, 340–354, doi:10.1175/1520-0426-19.3.340.

——, T. J. Schuur, D. W. Burgess, P. L. Heinselman, S. E. Giangrande, and D. S. Zrnić, 2005a: The joint polarization experiment: Polarimetric rainfall measurements and hydrometeor classification. *Bull. Amer. Meteor. Soc.*, **86**, 809–824, doi:10.1175/BAMS-86-6-809.

——, ——, ——, and D. S. Zrnić, 2005b: Polarimetric tornado detection. *J. Appl. Meteor.*, **44**, 557–570, doi:10.1175/JAM2235.1.

Shupe, M. D., and Coauthors, 2008: A focus on mixed-phase clouds: The status of ground-based observational methods. *Bull. Amer. Meteor. Soc.*, **89**, 1549–1562, doi:10.1175/2008BAMS2378.1.

Straka, J. M., D. S. Zrni, and A. V. Ryzhkov, 2000: Bulk hydrometeor classification and quantification using polarimetric radar data: Synthesis of relations. *J. Appl. Meteor.*, **39**, 1341–1372, doi:10.1175/1520-0450(2000)039<1341:BHCAQU>2.0.CO;2.

Tatarinov, V. N., and S. V. Tatarinov, 2011: A statistical theory of the electromagnetic field polarization parameters at the scattering by distributed radar objects. *Wave Propagation*, A. Petrin, Ed., InTech, 513–538 pp.

Vig, J. R., 1992: Introduction to quartz frequency standards. Revision 1, Army Research Laboratory Research and Development Tech. Rep. SLCET-TR-92-1, 56 pp. [Available online at www.dtic.mil/dtic/tr/fulltext/u2/a256373.pdf.]

Wolde, M., and G. Vali, 2001a: Polarimetric signatures from ice crystals observed at 95 GHz in winter clouds. Part I: Dependence on crystal form. *J. Atmos. Sci.*, **58**, 828–841, doi:10.1175/1520-0469(2001)058<0828:PSFICO>2.0.CO;2.

——, and ——, 2001b: Polarimetric signatures from ice crystals observed at 95 GHz in winter clouds. Part II: Frequencies of occurrence. *J. Atmos. Sci.*, **58**, 842–849, doi:10.1175/1520-0469(2001)058<0842:PSFICO>2.0.CO;2.

Zrnić, D. S., and A. V. Ryzhkov, 1998: Observations of insects and birds with a polarimetric radar. *IEEE Trans. Geosci. Remote Sens.*, **36**, 661–668, doi:10.1109/36.662746.

——, R. Doviak, G. Zhang, and A. Ryzhkov, 2010: Bias in differential reflectivity due to cross coupling through the radiation patterns of polarimetric weather radars. *J. Atmos. Oceanic Technol.*, **27**, 1624–1637, doi:10.1175/2010JTECHA1350.1.